SUPPORTING INFORMATION FOR

Cu(II)-Doped $Cs_2SbAgCl_6$ Double Perovskite: A Lead-Free, Low-Bandgap Material

Abhoy Karmakar,[1] Mya S. Dodd,[1] Satyam Agnihotri,[1] Enrico Ravera,[2] and Vladimir K. Michaelis[1]*

1-Department of Chemistry, University of Alberta, Edmonton, Alberta T6G 2G2, Canada

2-Magnetic Resonance Center (CERM), University of Florence and Consorzio Interuniversitario Risonanze Magnetiche di Metalloproteine, Via L. Sacconi 6, 50019 Sesto Fiorentino (FI), Italy and Department of Chemistry "Ugo Schiff", University of Florence, Via della Lastruccia 3, 50019 Sesto Fiorentino (FI), Italy

* Corresponding author: Tel: +1-780-248-5893; email: vladimir.michaelis@ualberta.ca

TABLE OF CONTENTS

EXPERIMENTAL

Materials and Methods

All starting precursor materials and solvents were obtained from commercial sources and used without further purification: CsCl (>99%, Acros Organics, NJ, USA), Sb_2O_3 (99%, Sigma Aldrich Co., St. Louis, MO, USA), $AgNO_3$ (EM Science, NJ, USA), $CuCl_2 \cdot 2H_2O$ (Aldrich Chemical Company, Inc, USA), HCl (EMD Chemical Inc., Darmstadt, Germany), H_3PO_2 (50 wt. % in H_2O, Sigma-Aldrich Co., St. Louis, MO, USA). All reactions were performed under ambient conditions.

Synthesis of Polycrystalline $Cs_2SbAgCl_6$

Freshly prepared AgCl was used in this synthesis. AgCl was formed by adding 10 M HCl (in excess) to an aqueous solution of $AgNO_3$, resulting in the precipitation of a white solid, which was filtered using a Buchner funnel, washed with 95% ethanol and dried under suction filtration. First, 4 mL of 10 M HCl and 1 mL of H_3PO_2 solvent were placed into a vial and heated to 120 °C using a hot plate with gentle stirring using a magnetic stir bar. Then 0.5 mmol of solid Sb_2O_3 (0.146 g) and 1 mmol of freshly prepared AgCl (0.143 g) were added to the hot solvent mixture, followed by the addition of 2 mmol of CsCl (0.337 g); immediately, a pale-yellow precipitate was observed (later confirmed via PXRD and EDX to be $Cs_2SbAgCl_6$). The mixture was heated for one hour and then left at room temperature for two hours. The polycrystalline solid was filtered using a Buchner funnel and washed with 95% ethanol, followed by overnight drying. We note that a small amount of $Cs_3Sb_2Cl_9$ can form as an impurity during the synthesis as shown in Figure S15.

Synthesis of Polycrystalline $Cs_2Sb_{1-a}Ag_{1-b}Cu_{2x}Cl_6$ (a+b = 2x, x = 0.01, 0.05, and 0.10)

AgCl was prepared as described above.

For x = 0.01: 0.034 g of $CuCl_2•2H_2O$ (0.20 mmol) was dissolved in 5 mL of 10 M HCl and a homogeneous solution was obtained. In a separate reaction, 10 mL of 10 M HCl was placed into a vial and heated to 120 °C with gentle stirring using a hot plate equipped with a magnetic stirrer. 1 mmol of white solid Sb_2O_3 powder (0.292 g) and 2 mmol of freshly prepared AgCl (0.287 g) were dissolved in the hot solvent mixture. Following dissolution, 4 mmol of CsCl (0.673 g) and 0.04 mmol (corresponding to 0.0068 g or 1 mL solution) of $CuCl_2•2H_2O$, prepared as described above, were added to the solution. A black precipitate was immediately observed. The mixture was heated for one hour and then left at room temperature for two hours. The polycrystalline solid was filtered using a Buchner funnel, washed with 95% ethanol, and followed by overnight drying.

For x = 0.05, 0.10: 10 mL of 10 M HCl was placed into a vial with gentle stirring and heated to 120 °C using a hot plate equipped with a magnetic stir bar. 0.95 mmol (0.277 g) or 0.90 mmol (0.262 g) of white solid Sb_2O_3 powder and 1.9 mmol (0.272 g) or 1.8 mmol (0.258 g) of freshly prepared AgCl, for x = 0.05 and 0.10, respectively, were dissolved in the hot solvent mixture. Following dissolution, 4 mmol of CsCl (0.673 g) and 0.2 mmol (0.034 g) or 0.4 mmol (0.068g) of $CuCl_2•2H_2O$, for x = 0.05 and 0.10, respectively, were added to the solution. Immediately following this step, a black precipitate was observed. The mixture was heated for one hour and then allowed to stand at room temperature for two hours. The polycrystalline solid was filtered using a Buchner funnel, washed with 95% ethanol, and allowed to dry overnight.

Diffuse Reflectance (DR) Spectroscopy

A Cary 5000 UV−Vis−NIR spectrophotometer, equipped for the analysis of small-quantity fine powdered samples, was used to obtain DR data (Analytical and Instrumental Laboratory, University of Alberta). Each sample was packed into a black boat (~100 mg/sample) and each measurement was acquired between the wavelengths of 2500 and 200 nm.

The diffuse reflectance spectra were converted to pseudo-absorbance spectra using the following Kubelka-Munk transformation:[5] $\alpha \sim \frac{(1-R)^2}{2R}$, where, R = absolute reflectance and α = pseudo-absorbance. The direct and indirect bandgaps were measured by taking the intercept upon extrapolation of the linear regions of $(\alpha h\nu)^2$ vs E(eV) and $(\alpha h\nu)^{1/2}$ vs E(eV) plots, respectively.

Powder X-Ray Diffraction (PXRD)

Powder X-ray diffraction (PXRD) measurements were collected on an Inel MPD multi-purpose diffractometer (40 kV, 50mA) system (Department of Chemistry, University of Alberta) equipped with a CPS 120 curved position sensitive X-ray detector and Cu K_α radiation source (1.540596 Å). Samples were placed on a plastic sample holder and 2θ data were collected from 0.290° to 113.767° with a step increment of 0.029°.

Energy Dispersion X-Ray (EDX) Measurements

The energy dispersive X-ray (EDX) analysis was performed using a low vacuum JEOL JSM-6010LA InTouchScope (Scanning Electron Microscope Laboratory, University of Alberta), equipped with the latest Bruker Silicon Drift Detector.

Inductively Coupled Plasma-Optical Emission Spectrometric (ICP-OES) Measurements

The inductively coupled plasma-optical emission spectrometric (ICP-OES) analysis was performed using a Argon plasma ICP spectrophotometer Perkin Elmer Optima 2000 OES DV (Laboratorio di Microanalisi, University of Florence) instrument. The samples were dissolved in *aqua regia.*

Thermogravimetric Analysis (TGA)

Thermogravimetric analysis was performed using a Perkin Elmer Pyris 1 instrument (Analytical and Instrumental Laboratory, University of Alberta) with a nitrogen gas flow of 20 mL/min and a heating rate of 5 °C/min. The temperature range was 25-800 °C.

Humidity and Thermal Stress Tests

A small amount of freshly prepared $Cs_2SbAgCl_6$ (x = 0.00) and highest Cu^{2+}-doped (x = 0.10) materials were placed in a custom-built humidifying chamber at 55 ± 5% relative humidity at 295 K (Figure S12). The samples were placed in a fume hood within this chamber in the presence of normal laboratory light (natural and artificial). After one year (x = 0.00) or one month (x = 0.10), the samples were removed from the humidifying chamber, and further analyses including, PXRD, ^{133}Cs MAS NMR, and DR were collected.

A small amount of freshly prepared $Cs_2SbAgCl_6$ (x = 0.00) and highest Cu^{2+} doped (x = 0.10) materials were placed in an oven at approximately 110 °C for six days, then removed and placed on the bench to cool to ambient temperature. Samples were then analyzed by PXRD, ^{133}Cs MAS NMR spectroscopy and DR experiments to confirm purity and stability of the samples.

Electron Paramagnetic Resonance (EPR) Spectroscopy

EPR spectra were acquired at X-band (9.77 GHz) on a Bruker ELEXSYS spectrometer (CERM, University of Florence), equipped with a standard ST4102 cavity. Field modulation was 20 G at 100 kHz and four scans were taken for each sample under ambient conditions. MW power was set to 50 mW; no evidence of saturation was observed.

Solid-State Nuclear Magnetic Resonance (NMR) Spectroscopy

^{121}Sb NMR: Antimony-121 NMR spectra were acquired at 7.05 T (300 MHz, ^{1}H) and 11.75 T (500 MHz, ^{1}H) on Bruker Avance 300 and 500 NMR spectrometers, respectively, using a non-selective Bloch pulse (short tip angle) or a selective (1.3 μs $\pi/2$, $\gamma B_1/2\pi$ = 65 kHz) Hahn-echo pulse sequence ($(\pi/2)_x - \tau_1 - (\pi)_y - \tau_2 -$ ACQ, where τ_1 and τ_2 represent the inter-pulse and refocusing delays, respectively), 1,000 to 29,000 co-added transients and a recycle delay of 2 s. Samples were packed in 4 mm OD ZrO_2 rotors (80 μL fill volume) and spectra were acquired under non-spinning and magic-angle spinning (MAS) conditions with a spinning frequency between 10 and 12 kHz. Additional ^{121}Sb NMR spectra were acquired at 21.1 T (900 MHz, ^{1}H) on a Bruker Avance II 900 NMR spectrometer using a 4 mm H/X MAS Bruker probe and a modified solid-echo pulse sequence ($(\pi/2)_x - \tau_1 - (\pi)_y - \tau_2 -$ ACQ),[6-8] $\gamma B_1/2\pi$ = 83 kHz (1.0 μs $\pi/2$,), 1,024 co-added transients and a recycle delay of 2 s. All ^{121}Sb NMR spectra were referenced by setting the peak for 0.5 M $KSbF_6$ to δ = 0.00 ppm.[1,2]

^{133}Cs NMR: Cesium-133 NMR spectra of the $Cs_2SbAgCl_6$ parent (x = 0.00) and of the Cu^{2+}-doped (0.01, 0.05, and 0.10) materials were acquired at 11.75 T (500 MHz ^{1}H) on a Bruker Avance 500 NMR spectrometer, with a Bloch pulse using a short pulse (1.25 μs, $\gamma B_1/2\pi$ = 50 kHz), 64 to 512 co-added transients and a recycle delay between 60 and 500 s. Samples were packed in 4 mm OD ZrO_2 rotors and spectra were collected under MAS conditions ($\omega_r/2\pi$ = 13 kHz). Variable temperature NMR

spectra were acquired at 238, 291, 323, and 343 K using appropriate relaxation delays (determined using a saturation recovery pulse sequence) to obtain pseudo-quantitative spectra (some paramagnetic quenching is likely due to the presence of Cu^{2+}). The sample and probe temperature were permitted to stabilize for 10-15 minutes prior to each VT data point acquisition. The temperatures were calibrated with ^{207}Pb NMR using $MAPbCl_3$.[3] Cesium-133 NMR spectra of Cu^{2+} doped $Cs_2SbAgCl_6$ materials (x = 0.01, 0.05, and 0.10) were acquired at 21.1 T (900 MHz ^1H) on a Bruker Avance II 900 spectrometer using a 2.5 mm H/X MAS Bruker probe and a solid pulse (1.0 μs π/4 pulse) with 10 s recycle delays. Samples were packed in 2.5 mm OD ZrO_2 rotors and spectra were collected using a spinning frequency of 30 kHz. ^{133}Cs 2D exchange spectroscopy (EXSY)[9] spectra were acquired at a spinning frequency of 30 kHz with π/2 pulses of 2.0 μs, recycle delays of 5 s, 96 to 128 co-added transients and 128 t_1 increments; mixing times ranged from 0.1 ms to 1 sec (Figure S13). All ^{133}Cs NMR spectra were referenced by setting the ^{133}Cs peak of a 0.1 M CsCl solution to $\delta = 0.00$ ppm.

Table S1. Nominal and elemental analyzed results (EDX, ICP-OES and ^{133}Cs NMR) for $Cs_2SbAgCl_6$ (x = 0.00) and for the Cu^{2+}-doped (x = 0.01, 0.05, 0.10) materials.

x[a]	Atom% by EDX[b]					Cu Composition				
	Cs	Sb	Ag	Cl	Cu	Nominal (atomic ratio %) Cu/Cs	Nominal (atomic ratio %) Cu/Sb	ICP-OES[c] (atomic ratio %) Cu/Cs	ICP-OES[c] (atomic ratio %) Cu/Sb	^{133}Cs NMR % Cu_{2x}[d] (± 0.5)
0.00	21.64 (0.93)	11.24 (0.63)	9.72 (0.74)	57.40 (0.90)	-	-	-	--	--	-
0.010	21.04 (0.42)	11.07 (0.54)	10.31 (0.14)	56.84 (1.05)	0.74 (0.46)	1.00	2.00	0.55	1.07	0.43
0.050	21.84 (0.74)	11.12 (0.47)	8.78 (0.72)	57.18 (0.78)	1.08 (0.69)	5.00	10.53	1.52	3.48	2.54
0.100	22.12 (0.71)	11.19 (0.60)	6.80 (0.51)	58.33 (1.20)	1.55 (0.94)	10.00	22.22	2.53	6.09	3.94

[a] x is the nominal Cu^{2+} composition in $Cs_2Sb_{1-a}Ag_{1-b}Cu_{2x}Cl_6$.

[b] EDX is energy-dispersive X-ray spectroscopic analysis (in quintuplicate).

[c] ICP-OES is inductively coupled plasma- optical emission spectrometric analysis (in triplicate).

[d] Cu_{2x} is % Cu^{2+} concentration in the final product of $Cs_2Sb_{1-a}Ag_{1-b}Cu_{2x}Cl_6$ from ^{133}Cs NMR.

Please note: Uncertainties are provided in the parentheses, as the dopant concentrations are near the detection limits, hence the larger uncertainties. Figure S9 shows a nearly linear relationship between quantitatively measured Cu concentrations and the Cu/Sb atomic ratio by synthetic loading (nominal composition). Due to the low Cu concentrations and associated challenges in elemental analysis of these materials, we refer to all Cu-doped materials via their nominal composition, x.

Table S2. ^{133}Cs and ^{121}Sb NMR relaxation parameters (T_1 and T_2*) for $Cs_2SbAgCl_6$ (x = 0.00) and for the x = 0.10 Cu^{2+}-doped materials. All ^{133}Cs NMR relaxation parameters (T_1 and T_2*) were measured at 11.75 T and whereas all ^{121}Sb NMR relaxation parameters (T_2*) were measured at 7.05 T.

x	^{133}Cs (T_1), sec	^{133}Cs (T_2*), ms	^{121}Sb (T_2*), µs
0	51 ± 6	6 ± 1	360 ± 40
0.10	2.7 ± 0.5	1.3 ± 0.1	130 ± 30

Table S3. Calculated contributions from the three ^{133}Cs MAS NMR peaks (Peak-1, Peak-2, and Peak-3) and the fitted line equations.

^{133}Cs NMR Peak	Area % for x (± 1 %)				Fitted Linear Equation
	0.00	**0.01**	**0.05**	**0.10**	
Peak-1	100	97.4	79.8	67.5	$\delta_{iso}(^{133}Cs)$ / ppm = −334(32) x + 100(2); R^2 = 0.973
Peak-2	0	2.5	19.1	29.6	$\delta_{iso}(^{133}Cs)$ / ppm = 305(34) x + 1(2); R^2 = 0.963
Peak-3	0	0.2	1.1	2.9	$\delta_{iso}(^{133}Cs)$ / ppm = 29(3) x + 0(0); R^2 = 0.971

Table S4. FWHM values for ^{133}Cs MAS NMR spectra (Peak-1 and Peak-2 of Figure S5) for $Cs_2SbAgCl_6$ without or with Cu^{2+} doping, acquired at 11.75 T, T = 291 K and a spinning frequency of 13 kHz.

Cu^{2+} composition (x)	FWHM (Hz)	
	Peak-1	**Peak-2**
0.00	200(5)	-
0.01	205(5)	1350(20)
0.05	615(10)	1360(10)
0.10	770(10)	1350(10)

Table S5. FWHM values of ^{133}Cs MAS NMR spectra ($B_\circ$=21.1 T, $\omega_r/2\pi$ = 30 kHz) for $Cs_2SbAgCl_6$ (Figure S6).

Cu^{2+} composition (x)	FWHM (Hz)		
	Peak-1	**Peak-2**	**Peak-3**
0.01	305(5)	1625(25)	–
0.05	1035(10)	2080(20)	2500(200)
0.10	1410(10)	2310(20)	2700(100)

Table S6. Temperature dependence of chemical shifts and fitted line equations for Peak-1, Peak-2, and Peak-3 of the ^{133}Cs MAS NMR spectra for the Cu^{2+}-doped material (x = 0.10); acquired at 11.75 T with a spinning frequency of 13 kHz.

$\delta_{iso}(^{133}Cs)$	Temperature (T/K)				Fitted Linear Equation
	238	291	323	343	
Peak-1	77	82	84	85	$\delta_{iso}(^{133}Cs)$ / ppm = −6.3 (1000/T) + 102.9; R^2 = 0.999
Peak-2	−34	−13	−3	3	$\delta_{iso}(^{133}Cs)$ / ppm = −30.9 (1000/T) + 89.9; R^2 = 0.999
Peak-3	−147	−105	−87	−74	$\delta_{iso}(^{133}Cs)$ / ppm = −60.4 (1000/T) + 95.4; R^2 = 0.998

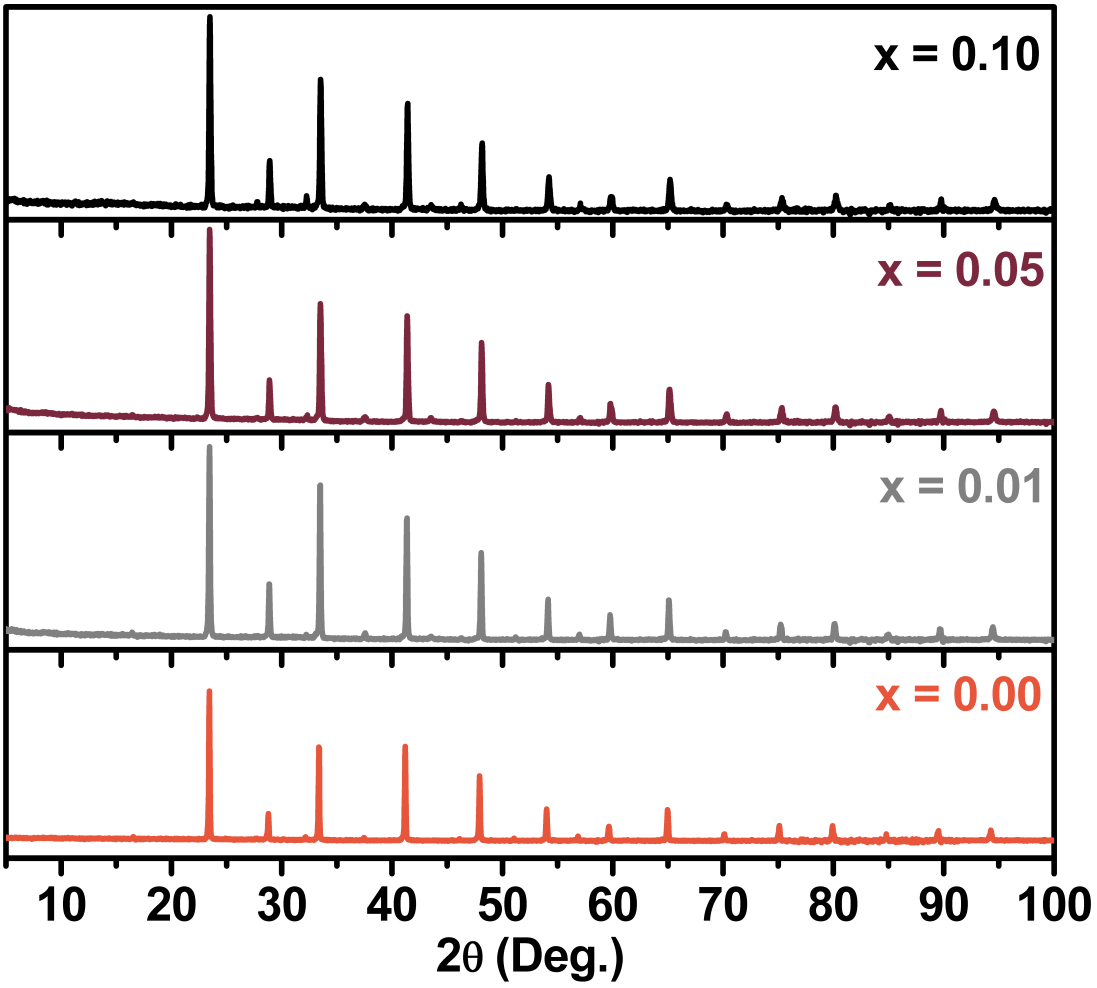

Figure S1: Enlargement of powder XRD patterns for $Cs_2SbAgCl_6$ (x = 0.00) and for Cu^{2+}-doped $Cs_2SbAgCl_6$ materials.

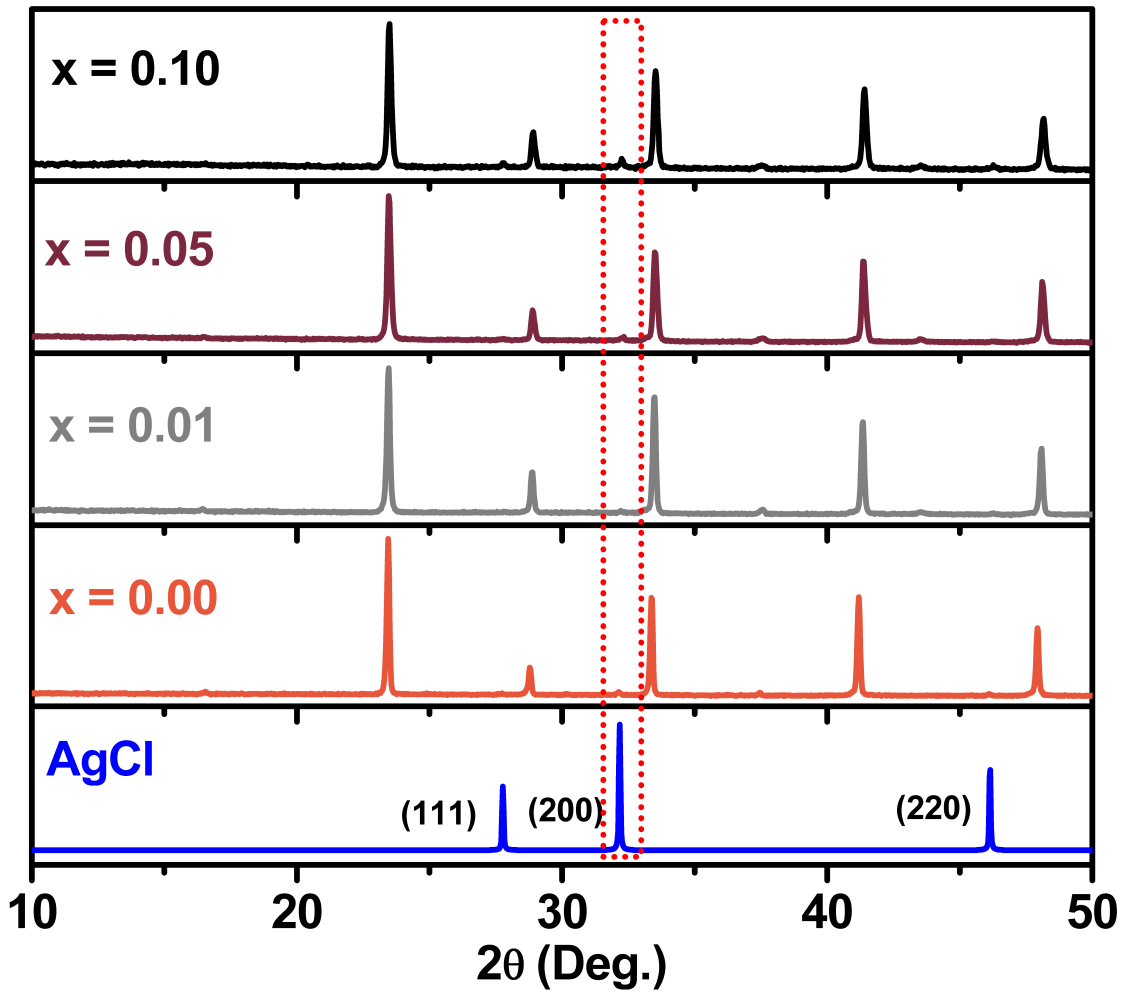

Figure S2: Powder XRD patterns for AgCl, $Cs_2SbAgCl_6$ and for the latter with the indicated level of nominal Cu^{2+} doping. The presence of AgCl in the double perovskite materials is indicated, with the relative intensity of the AgCl (200) peak increasing as the Cu^{2+} doping increases (dotted red box). Please note that the PXRD pattern for AgCl is simulated.[4]

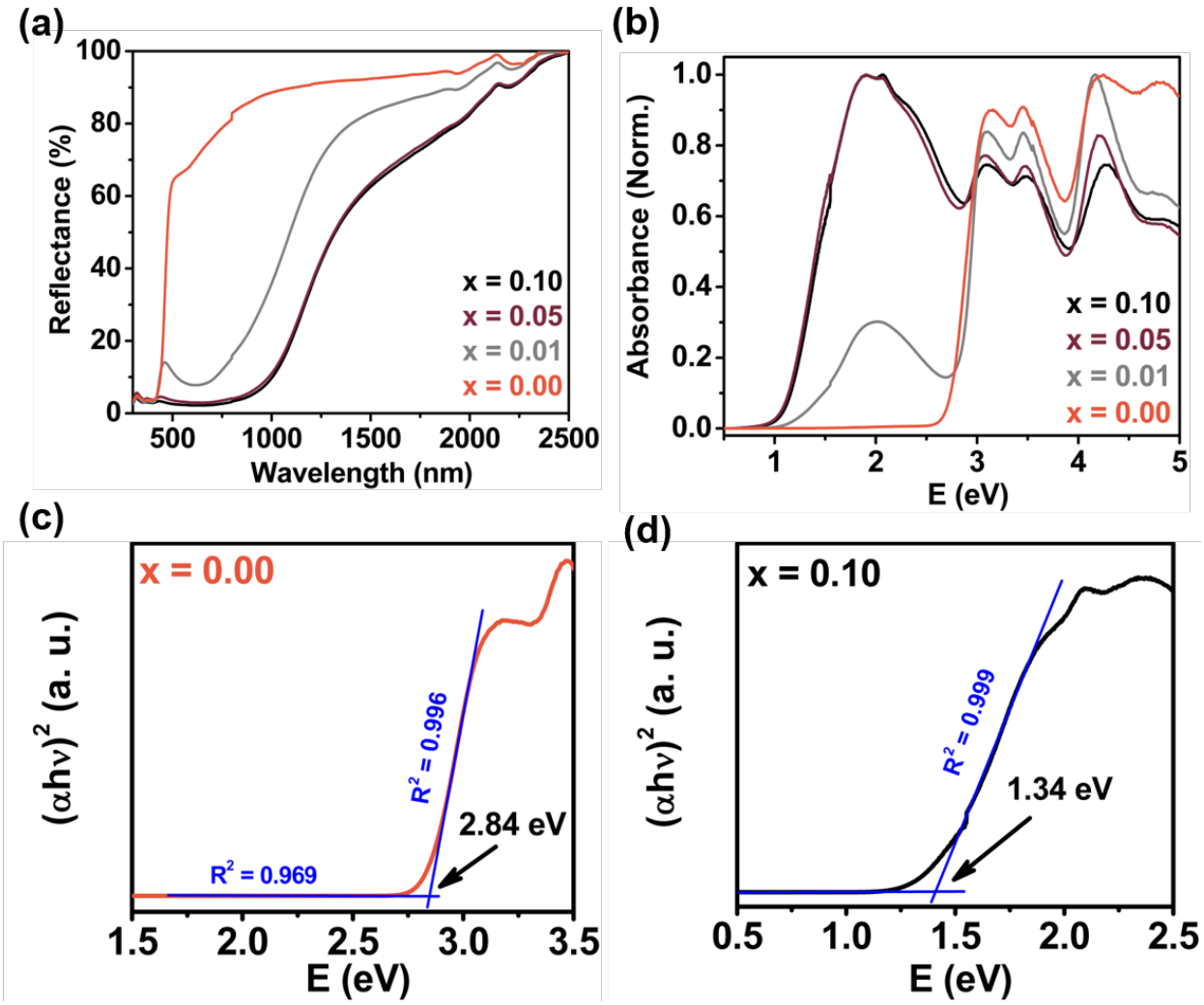

Figure S3. UV-VIS-NIR DR (a), and normalized absorption (b) spectrum for $Cs_2SbAgCl_6$ parent (i.e. x = 0.00) and all Cu^{2+}-doped (x = 0.01, 0.05, and 0.10) materials. The DR spectra is converted to absorbance by using the Kubelka-Munk equation (see Materials and Methods). The Tauc plots, which yield, assuming a direct allowed transition, bandgaps of 2.84 eV for $Cs_2SbAgCl_6$ (x = 0.00) (c), and 1.34 eV for the maximum Cu^{2+} doped material (x = 0.10) (d).

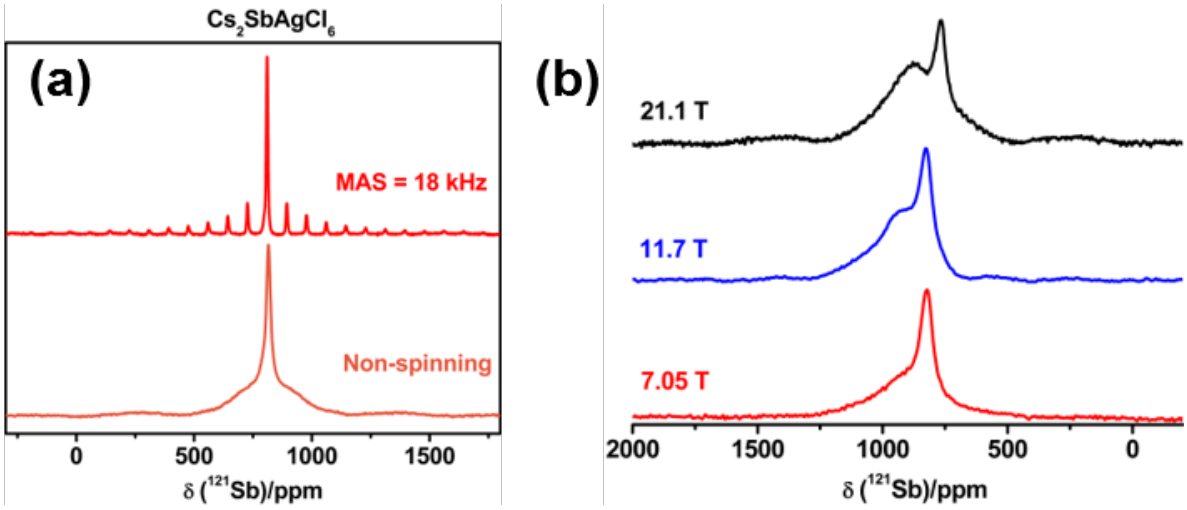

Figure S4. Comparison of ^{121}Sb NMR spectra of $Cs_2SbAgCl_6$ parent under non-spinning and magic-angle spinning (18 kHz) conditions at 21.1 T (a). Comparison of ^{121}Sb NMR spectra acquired at 7.05, 11.75, and 21.1 T for non-spinning $Cs_2SbAgCl_6$ with Cu^{2+} doping of x = 0.10, showing the improved Sb site resolution with increasing magnetic field strength. Data were acquired with a selective central transition pulse, optimized for the larger C_Q resonance to higher frequency (i.e. for the peak centred at ≈ 900 ppm) (b).

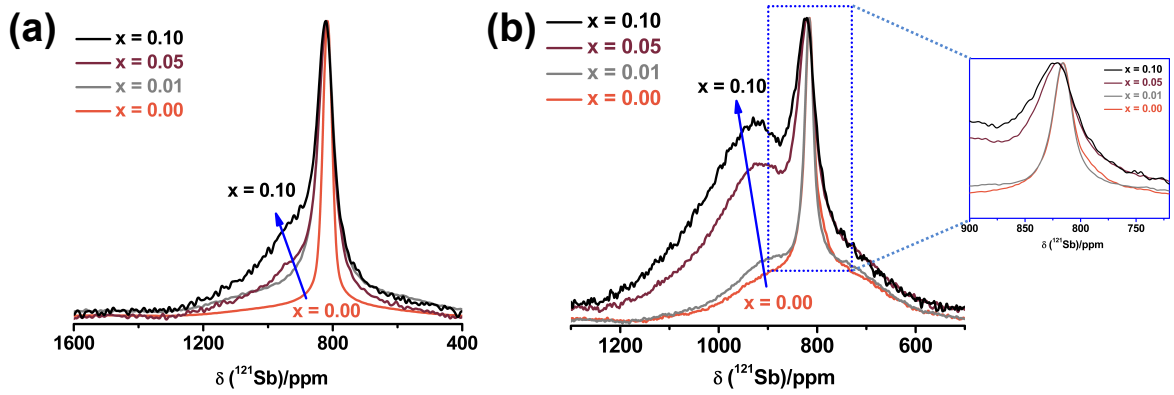

Figure S5. Comparison of ^{121}Sb NMR spectra acquired at 7.05 T (a) and 21.1 T (b) for non-spinning $Cs_2SbAgCl_6$ (x = 0.00) and for this material with Cu^{2+} doping (x = 0.01, 0.05, and 0.10), showing both the intensity of the high-frequency peak (δ ~ 900 ppm) and illustrating that the linewidth of the parent peak (i.e. the low frequency peak) increases with Cu^{2+} doping (insert).

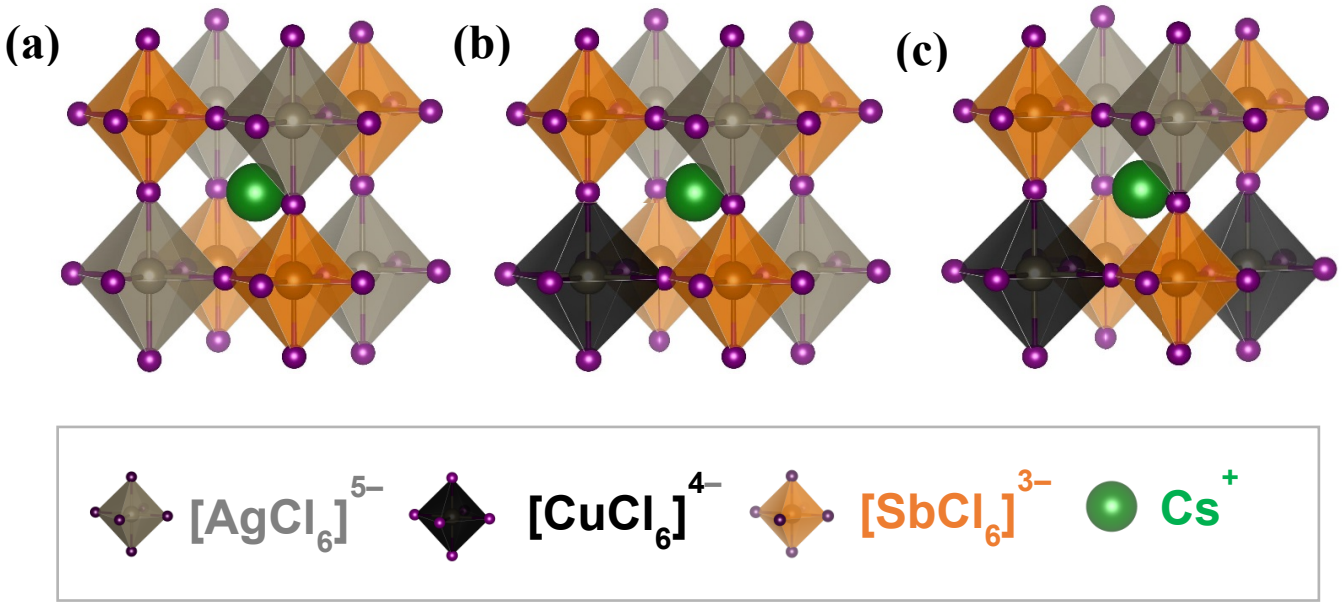

Figure S6: Schematic representation of $Cs_2SbAgCl_6$ double perovskites without (a), and with Cu^{2+} doping at one (b) or two (c) sites. This representation assumes that $[CuCl_6]^{4-}$ will generally only substitute $[AgCl_6]^{5-}$ sites (see the manuscript).

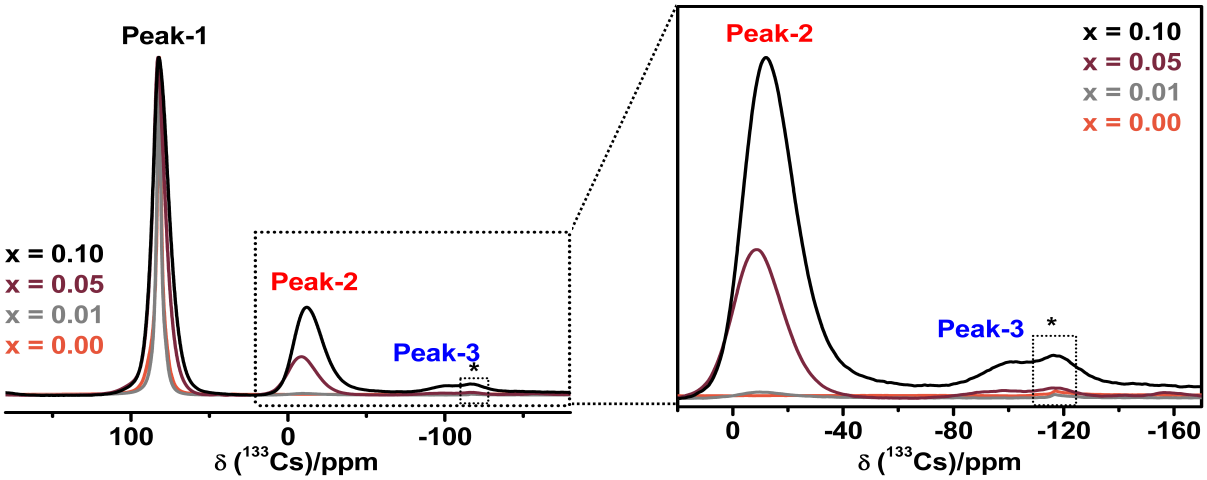

Figure S7: Comparison of ^{133}Cs MAS NMR spectra for $Cs_2SbAgCl_6$ without (x = 0.00) and with (x = 0.01, 0.05, and 0.10) Cu^{2+} doping, acquired at 11.75 T with a spinning frequency of 13 kHz, showing that the linewidth of Peak-1 increases with Cu^{2+} content (left), and that the relative intensities (with respect to the normalized Peak-1) of Peak-2 and Peak-3 increase with Cu^{2+} doping concentration (right). Spinning sidebands are indicated with an asterisk (*).

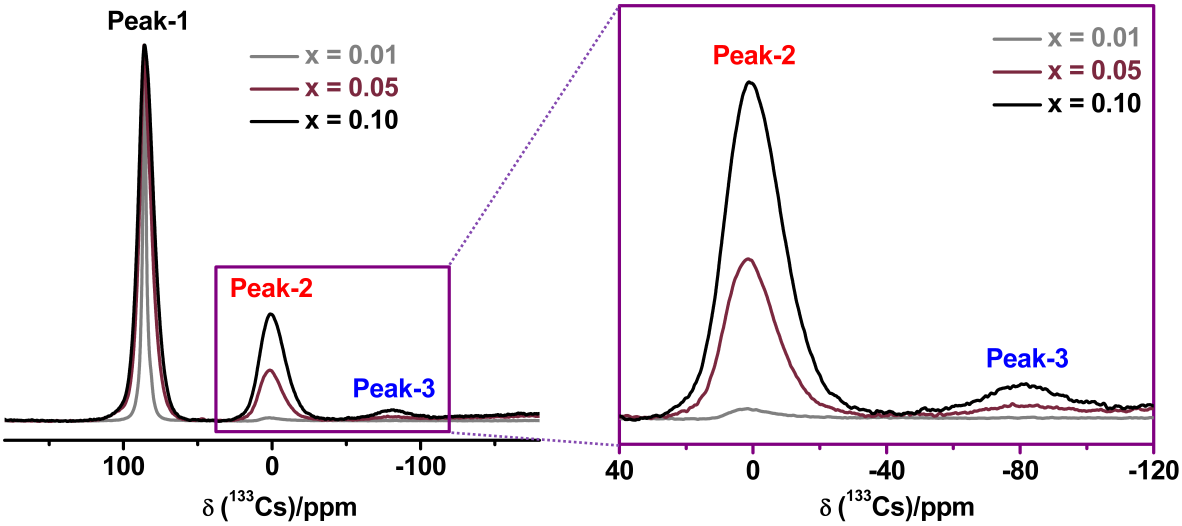

Figure S8. Comparison of ^{133}Cs MAS NMR spectra for $Cs_2SbAgCl_6$ with or without Cu^{2+} doping, acquired at 21.1 T with a spinning frequency of 30 kHz, showing that the linewidth of Peak-1 increases with Cu^{2+} content (left), and that the relative intensities (with respect to the normalized Peak-1) of Peak-2 and Peak-3 increase with Cu^{2+} doping content (right).

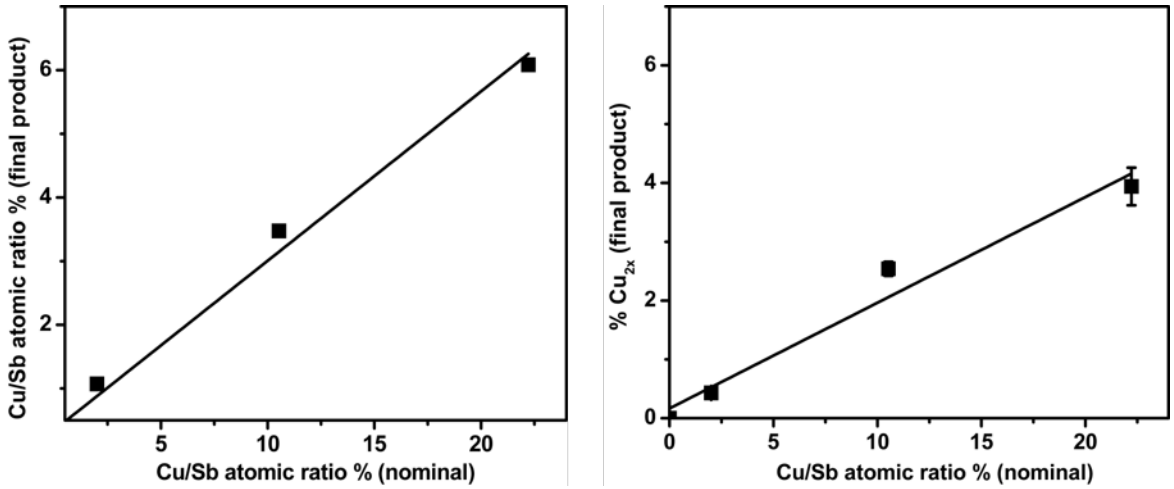

Figure S9: Linear relation of Cu/Sb atomic ratio % before (nominal) and after (final product) the synthesis based on the ICP-OES data (left) and Cu-composition based on ^{133}Cs MAS NMR spectra acquired at 11.75 T against nominal Cu/Sb atomic ratio % (right).

^{133}Cs NMR Analysis: From the crystal structure of $Cs_2SbAgCl_6$, the Cs^+ ion resides in the cubooctahedral void, surrounded by a total of eight (four Ag^+ and four Sb^{3+}) octahedral sites (Figure S6a). Similarly, each Ag^+ or Sb^{3+} site is also surrounded by eight Cs^+ ions. Since the peaks labeled Peak-2 in the ^{133}Cs NMR spectra arise from Cu^{2+} substitution in a Ag^+ site, each Cu^{2+} ion is surrounded by eight Cs^+ ions. If we neglect the minor contribution giving rise to Peak-3, then from the ^{133}Cs NMR spectra, the total Cu^{2+} concentration in the final product is given by Equation S1:

$$(2x) = \frac{1}{8} \times (\text{Area}/\%) \qquad \text{S1}$$

where Area/% refers to the percent contribution of Peak-2 to the total ^{133}Cs spectrum. For example, when x = 0.10, the area for Peak-2 in the ^{133}Cs NMR spectrum is 29.5 % and thus:

$$(2x) = (a+b) = \left(\frac{1}{8} \times 29.5\right)\% = 3.37\ \% = 0.037 \qquad \text{S2}$$

Hence, $x = \left(\frac{1}{2} \times 0.037\right) = 0.0185$.

Please note that the general formula of Cu^{2+} doped material is: $Cs_2Sb_{1-a}Ag_{1-b}Cu_{2x}Cl_6$ (a+b = 2x) and that the (2x) value represents the fraction of octahedral sites (Sb^{3+} or Ag^+) that are substituted by Cu^{2+} ions.

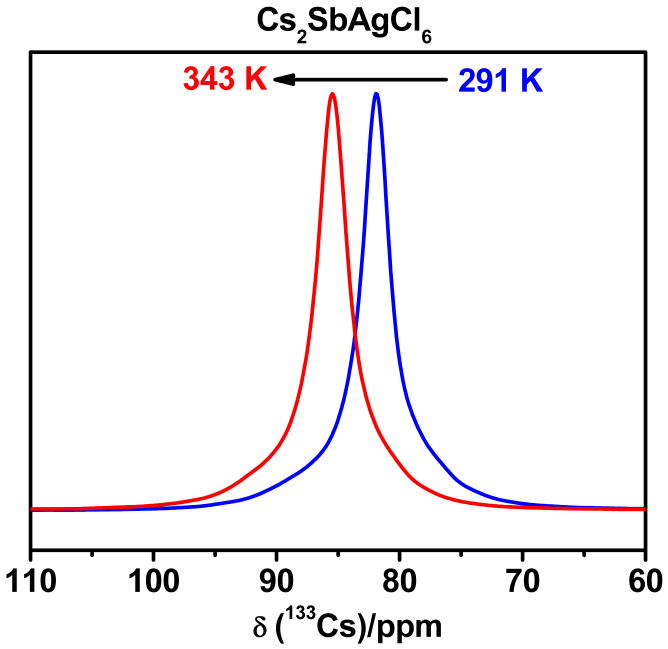

Figure S10. Temperature dependent ^{133}Cs MAS NMR spectra of $Cs_2SbAgCl_6$ parent.

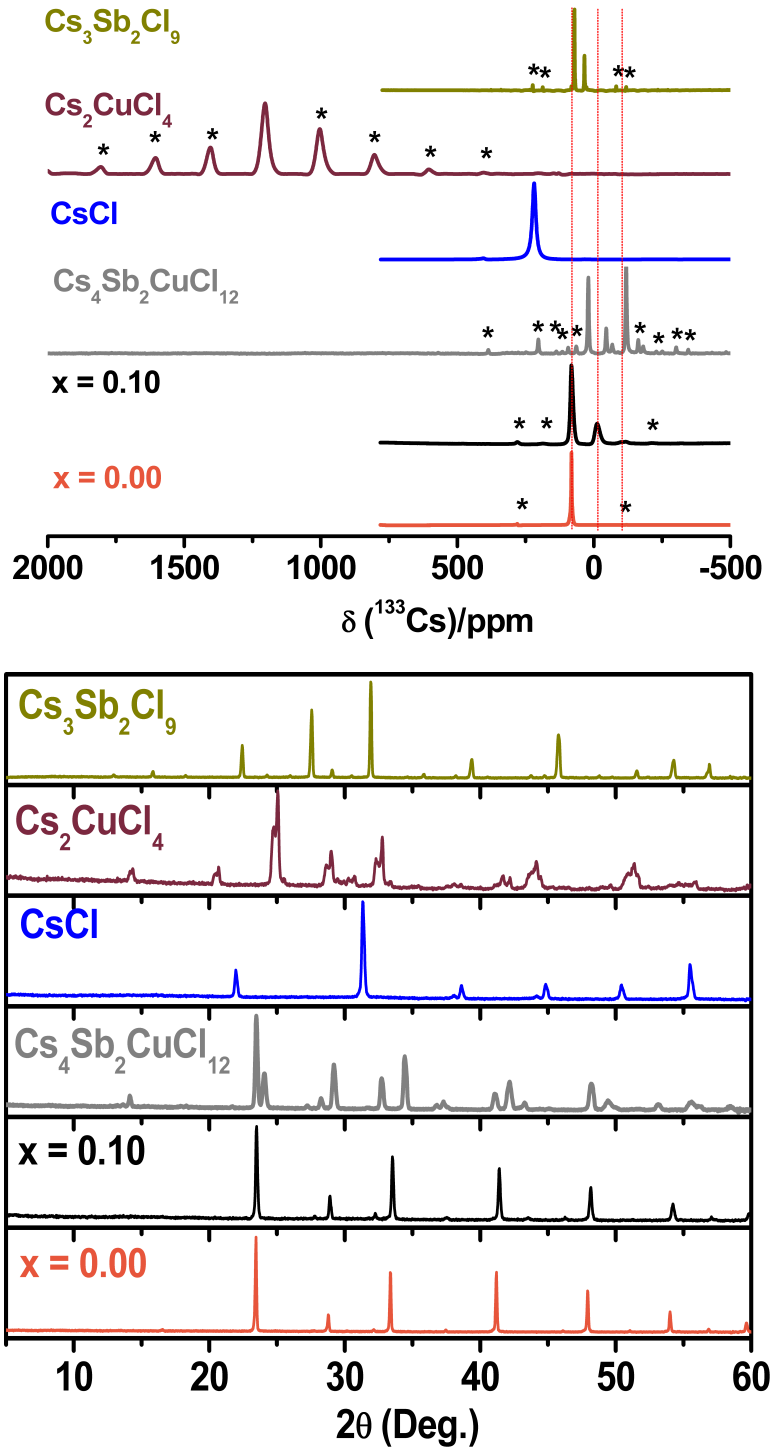

Figure S11. Cesium-133 MAS NMR spectra (B_o = 11.75 T, top) and PXRD patterns (bottom) for $Cs_2SbAgCl_6$ (x = 0.00 and 0.10), $Cs_4Sb_2CuCl_{12}$, CsCl, Cs_2CuCl_4 and $Cs_3Sb_2Cl_9$. The asterisks (*) indicate spinning sidebands.

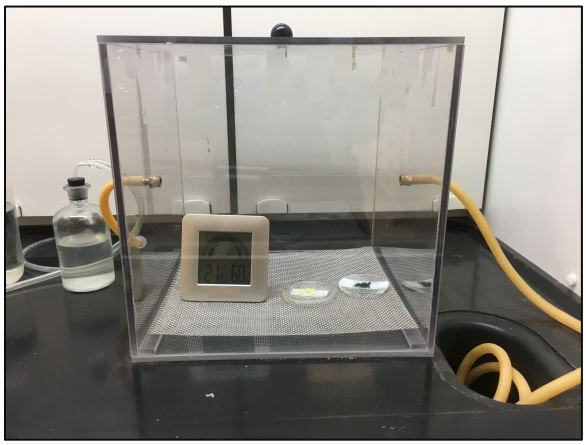

Figure S12. Photograph of the custom-built humidifying chamber.

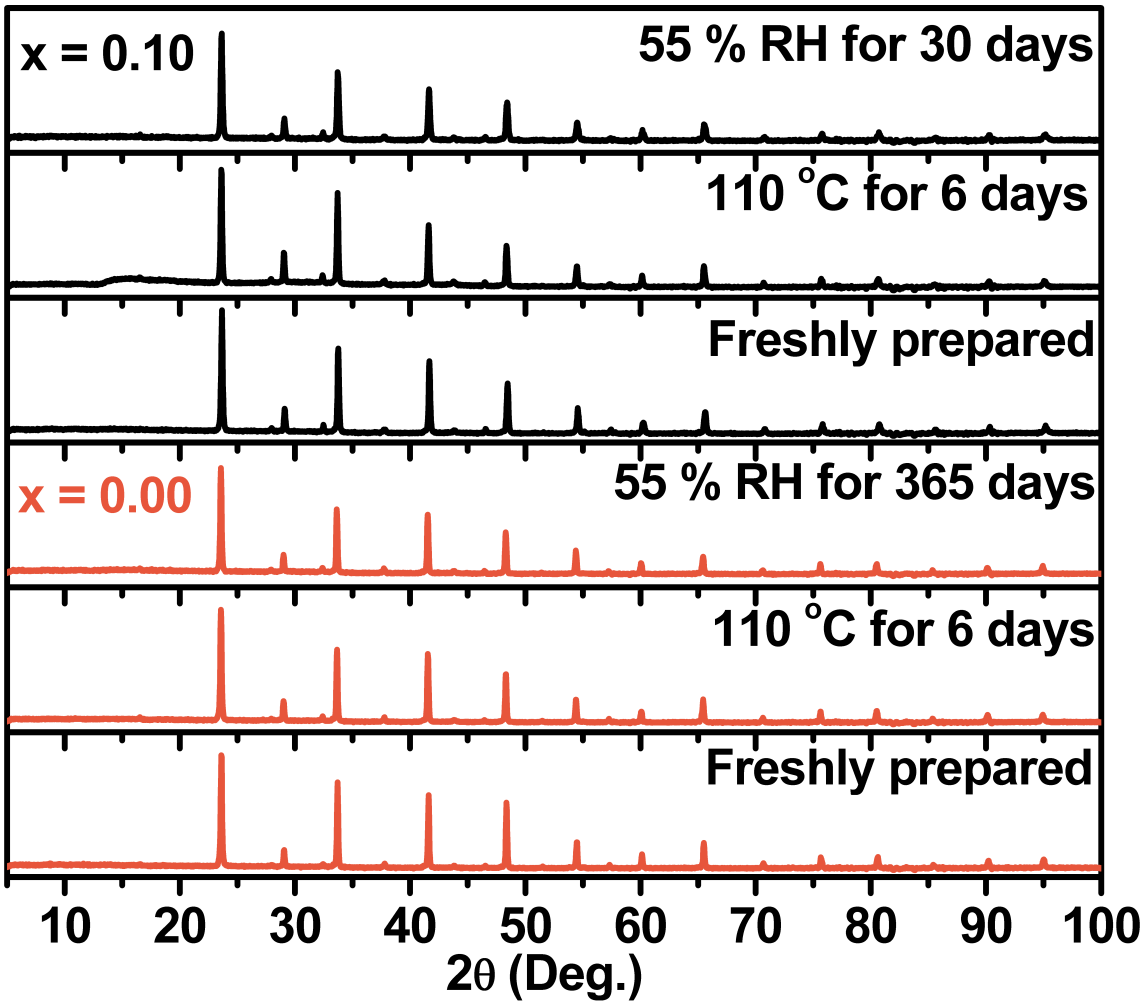

Figure S13. Enlarged version of powder XRD pattern for the stability experiments of $Cs_2SbAgCl_6$ parent (x = 0.00) and the maximum Cu^{2+}-doped (x = 0.10) materials under the indicated conditions.

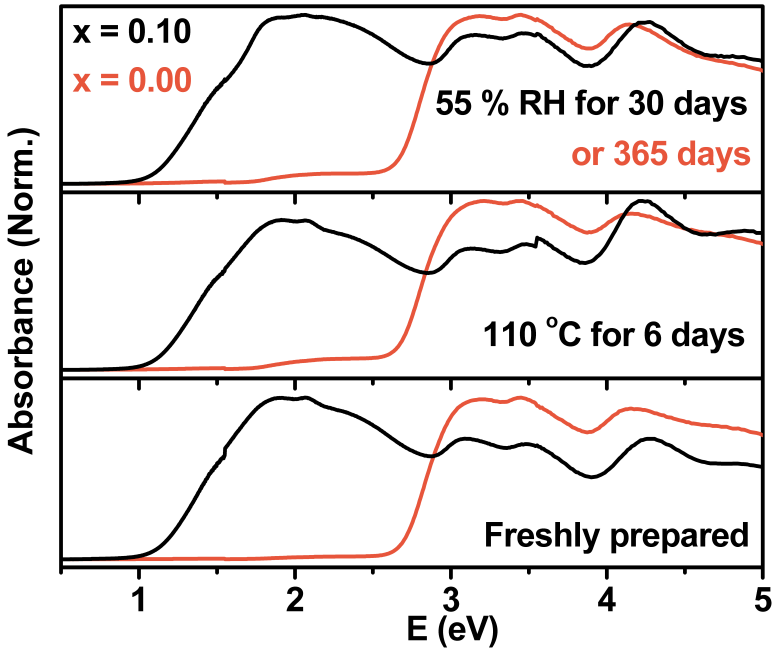

Figure S14. Absorption spectra of $Cs_2SbAgCl_6$ parent (x = 0.00, red) and the maximum Cu^{2+}-doped (x = 0.10, black) materials under the indicated conditions. The absorption spectra were extracted from DR data by using the Kubelka-Munk equation (see Materials and Methods).

Determination of the pseudocontact contribution*:* The pseudocontact contribution to the shift arises because of the interaction of the nuclear spin with the average magnetic moment of the paramagnetic center, which does not average to zero in the case when magnetic susceptibility of the metal center is anisotropic. It can be related to the magnetic susceptibility through the Kurland-McGarvey equation[10] and, for the case of S=1/2 spins, it can be directly related to the electron g-matrix from EPR:

$$\delta^{\mathrm{pc}} = \frac{1}{12\pi r^3}\frac{\mu_0\mu_{\mathrm{B}}^2 S(S+1)}{3kT}\left(g_{\parallel}^2 - g_{\perp}^2\right)(3cos^2\theta - 1)$$

Using $g_{\parallel} = 2.3$ and $g_{\perp} = 2.0$, at about 4.5 Å the expected PCS value is 1.2 ppm, to which a further contribution amounting to about 20% coming from the temperature independent paramagnetism could be added.[11]

^{121}Sb NMR lineshape analysis of $Cs_2SbAgCl_6$: Since ^{121}Sb has a large quadrupole moment (Q = -36.0 fm^2) and I = 5/2, the lineshape and breadth of the NMR spectra are often dominated by the quadrupolar interaction. However, for the parent $Cs_2SbAgCl_6$ material, the Sb sites are located at an octahedral position within a cubic space group such that the overall EFG would be expected to be zero. In practice, slight defects or distortions within the lattice may impact the symmetry about some ^{121}Sb nuclei, such that a quadrupolar interaction is detected despite the octahedral symmetry. Analysis of the spectra acquired under non-spinning and MAS conditions as well as at multiple field strengths assist in determining these interactions. Other anisotropic interactions that may contribute to the linewidth and shape include magnetic shielding anisotropy, and direct (dipolar) and indirect (J-coupling) spin-spin coupling. A small quadrupolar interaction of 1 MHz would lead to a 30 Hz second order broadening contribution at 21.1 T, while the non-spinning linewidth is 3.2 kHz. The linewidth remains nearly constant across three magnetic field strengths (B_o = 7.05, 11.75 and 21.1 T). Since magnetic shielding scales linearly with field and the second order quadrupole broadening is inversely related, these anisotropic interactions are negligible in their contribution (i.e. < 1 ppm). Magic-angle spinning reduces the linewidth by nearly 50% (1.5 kHz) to a FWHM of 1.8 kHz, indicating a contribution from heteronuclear dipole coupling between ^{121}Sb and $^{35/37}$Cl; the remaining MAS linewidth is attributed to indirect spin-spin coupling between ^{121}Sb (N.A. = 57.2 %) and the six coordinating $^{35/37}$Cl anions (^{35}Cl: N.A. = 75.8%, I = 3/2 and ^{37}Cl: N.A. = 24.2%, I = 3/2). The Gaussian-like ^{121}Sb peak is attributed to the complex splitting pattern arising from spin-spin coupling of ^{121}Sb to the two Cl isotopes, further complicated by the quadrupole coupling interaction expected for the Cl isotopes, which is expected to be significant since these nuclei are not in a high-symmetry position. Hence, a complex J-splitting pattern that is unresolved at 7.05 T is observed.[1]

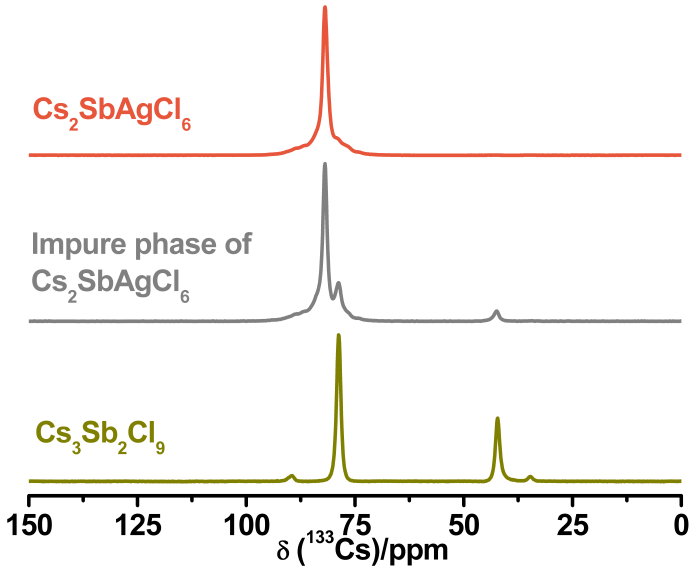

Figure S15. Cesium-133 MAS NMR spectra for $Cs_2SbAgCl_6$ and impure $Cs_2SbAgCl_6$ double perovskite and $Cs_3Sb_2Cl_9$.

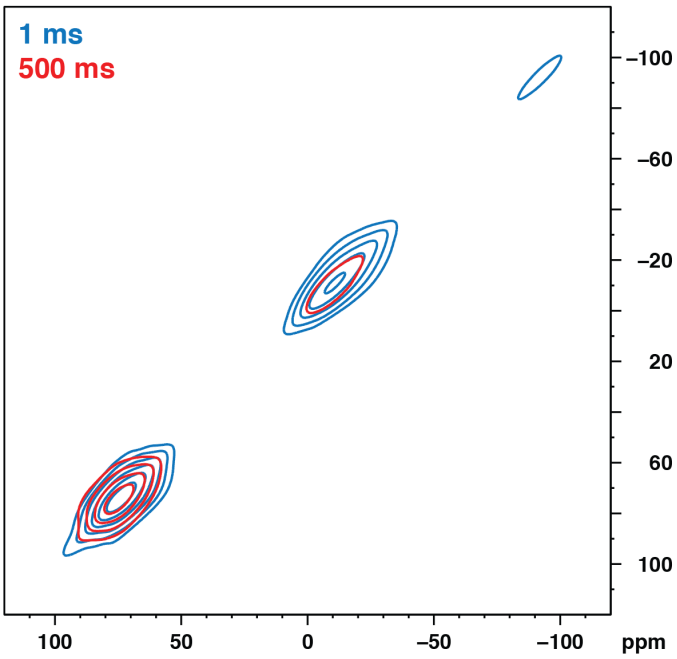

Figure S16. Two-dimensional ^{133}Cs EXSY NMR (B_o = 21.1 T; $\omega_r/2\pi$ = 30 kHz) contour plots of Cu^{2+}-doped $Cs_2SbAgCl_6$ (x = 0.10) with 1 ms (blue) and 500 ms (red) mixing times, showing no Cs exchange.

REFERENCES

(1) Faucher, A.; Terskikh, V. V; Wasylishen, R. E. Assessing Distortion of the AF_6 (A= As, Sb) Octahedra in Solid Hexafluorometallates (V) via NMR Spectroscopy. *Can. J. Chem.* **2015**, *93*, 938–944.

(2) Harris, R. K.; Becker, E. D.; de Menrzes, S. M. C.; Goodfellow, R.; Granger, P. Commission on Molecular Structure and Spectroscopy. *Pure Appl. Chem.* **2001**, *73*, 1795–1818.

(3) Bernard, G. M.; Goyal, A.; Miskolzie, M.; McKay, R.; Wu, Q.; Wasylishen, R. E.; Michaelis, V. K. Methylammonium Lead Chloride: A Sensitive Sample for an Accurate NMR Thermometer. *J. Magn. Reson.* **2017**, *283*, 14–21.

(4) Hull, S.; Keen, D. A. Pressure-Induced Phase Transitions in AgCl , AgBr , and AgI. *Phys. Rev. B* **1999**, *59*, 750–761.

(5) Kubelka, P.; Munk, F. Z. Ein Beitrag Zur Optik Der Farbanstriche. *Technol. Phys.* **1931**, *12*, 593-601.

(6) Mansfield, P. Multiple-Pulse Nuclear Magnetic Resonance Transients in Solids. *Phys. Rev.* **1965**, *137,* A961−A974.

(7) Bodart, P. R.; Amoureux, J. P.; Dumazy, Y.; Lefort, R. Theoretical and Experimental Study of Quadrupolar Echoes for Half-integer Spins in Static Solid State NMR. *Mol. Phys.* **2000**, *98*, 1545−1551.

(8) Davis, J. H.; Jeffrey, K. R.; Bloom, M.; Valic, M. I.; Higgs, T. P. Quadrupolar Echo Deuteron Magnetic Resonance Spectroscopy in Ordered Hydrocarbon Chains. *Chem. Phys. Lett.* **1976**, *42*, 390− 394.

(9) Jeener, J.; Meier, B. H.; Bachmann, P.; Ernst, R. R. Investigation of Exchange Processes by Two-dimensional NMR Spectroscopy. *J. Chem. Phys.* **1979,** *71*, 4546-4553.

(10) Kurland, R. J.; Mcgarvey, B. R. Isotropic NMR Shifts in Transition Metal Complexes: The Calculation of the Fermi Contact and Pseudocontact Terms. *J. Magn. Reson.* **1970**, *2*, 286–301.

(11) Walder, B. J.; Patterson, A. M.; Baltisberger, J. H.; Grandinetti, P. J. Hydrogen Motional Disorder in Crystalline Iron Group Chloride Dihydrates. *J. Chem. Phys.* **2018**, *149*, 084503.